Dendrimer-Templated Fe Nanoparticles for the Growth of Single-Wall Carbon Nanotubes by Plasma-Enhanced CVD

Placidus B. Amama,*,† Matthew R. Maschmann,†,‡ Timothy S. Fisher,†,‡ and Timothy D. Sands†,§

Birck Nanotechnology Center, School of Mechanical Engineering, School of Materials Engineering, School of Electrical and Computer Engineering, Purdue University, West Lafayette, Indiana 47907

Received: December 14, 2005; In Final Form: April 10, 2006

A fourth-generation (G4) poly(amidoamine) (PAMAM) dendrimer (G4-NH_2) has been used as a template to deliver nearly monodispersed catalyst nanoparticles to SiO_2/Si, Ti/Si, sapphire, and porous anodic alumina (PAA) substrates. Fe_2O_3 nanoparticles obtained after calcination of the immobilized Fe^{3+}/G4-NH_2 composite served as catalytic "seeds" for the growth of single-wall carbon nanotubes (SWNTs) by microwave plasma-enhanced CVD (PECVD). To surmount the difficulty associated with SWNT growth via PECVD, reaction conditions that promote the stabilization of Fe nanoparticles, resulting in enhanced SWNT selectivity and quality, have been identified. In particular, in situ annealing of Fe catalyst in an N_2 atmosphere was found to improve SWNT selectivity and quality. H_2 prereduction at 900 °C for 5 min was also found to enhance SWNT selectivity and quality for SiO_2/Si supported catalyst, albeit of lower quality for sapphire supported catalyst. The application of positive dc bias voltage (+200 V) during SWNT growth was shown to be very effective in removing amorphous carbon impurities while enhancing graphitization, SWNT selectivity, and vertical alignment. The results of this study should promote the use of exposed Fe nanoparticles supported on different substrates for the growth of high-quality SWNTs by PECVD.

Introduction

Carbon nanotubes[1] (CNTs) are materials of great interest because of their outstanding properties and suitability for a wide variety of applications.[2] The full technological potential of CNTs has been hindered somewhat by the difficulty associated with the control of their properties (selectivity, diameter, chirality, purity, and alignment). In recent years, significant research efforts have therefore concentrated on surmounting these barriers. The growth of single-wall carbon nanotubes (SWNTs) via chemical vapor deposition (CVD) offers an attractive means of controlling their properties because of the critical role played by catalyst nanoparticles. Although the growth mechanism of SWNTs in CVD is still unclear, several studies[3] have demonstrated that the size of the metal catalyst particle approximately determines the eventual diameter of the SWNT. Through the control of the size of the catalyst nanoparticles, it is possible to synthesize SWNTs of relatively uniform diameter.[3−5] Generally, SWNT selectivity is enhanced when sufficiently small nanoparticles (<5 nm),[6] appropriate catalysts,[7] carbon source,[8] and temperature[9] are used during CVD growth. Also of interest are key parameters such as the catalyst−substrate interaction and catalyst pretreatment, which have been used to increase SWNT selectivity and to control their properties.[10] It is therefore evident that during CVD growth of SWNTs, the catalyst material is probably the most significant parameter.

The precise control of the catalyst particle size distribution within the range selective for SWNT growth and the stabilization of the catalyst nanoparticles at high growth temperatures characteristic of CVD systems constitute major challenges. As a result of coarsening, SWNTs grown via CVD at higher substrate temperature generally tend to have a broader diameter distribution in comparison to those grown via laser ablation.[11] It is therefore necessary to develop methods for improving the stability and maintaining the monodispersity of catalyst nanoparticles in the CVD growth environment, especially in plasma-enhanced CVD. Nearly monodispersed metallic/bimetallic nanoparticles in the size range selective for SWNT growth have been synthesized by using dendrimers,[12] artificial ferritin,[6a] thermal decomposition of metal carbonyl complexes,[13] and metal−surfactant complexes.[14] Different supports such as MgO,[15] MCM-41,[16] and Al_2O_3 [17] have been successfully used to stabilize Fe nanoparticles at high CVD growth temperatures. In addition, the formation of Fe alloys with appropriate amounts of Mo,[18] Pt,[19] and Ru[17] inhibits coalescence of Fe nanoparticles and increases Fe stabilization resulting in increased SWNT selectivity, yield, and quality.

The use of dendrimers[12] as "nanotemplates" offers a reliable, flexible, and reproducible means of producing transition-metal nanoparticles of controlled size (less than a few nanometers), shape, and composition. The size of the metal particles can be controlled through appropriate choice of dendrimer generations or the metal ion−dendrimer ratio. As demonstrated by Dai and co-workers,[5] these nanocomposites can be immobilized on a solid support with ease via dip or spin coating and then calcined to remove the organic dendrimer, leaving behind exposed Fe_2O_3 nanoparticles that are then used as catalytic "seeds" for the growth of high-quality SWNTs.

Plasma-enhanced CVD (PECVD) is well suited to producing graphitized, vertically aligned, high-quality multiwall carbon nanotubes (MWNTs) and carbon nanofibers at low tempera-

* To whom correspondence should be addressed. E-mail: pamama@purdue.edu.

† Birck Nanotechnology Center, Purdue University.

‡ School of Mechanical Engineering, Purdue University.

§ School of Materials Engineering, School of Electrical and Computer Engineering, Purdue University.

10.1021/jp057302d CCC: $33.50
Published on Web 05/13/2006

tures.[20] The growth of SWNTs by PECVD has proven to be challenging based on previous reports[21] and our experience because it is difficult to maintain a low carbon supply in the PECVD growth environment. We recently accomplished the growth of high-quality SWNTs from a Co/Mo catalyst supported on nanoporous MgO through a systematic optimization of key reaction parameters.[22] Previous studies of the growth of SWNTs by PECVD for the most part involved the use of thin metal film catalyst or catalyst nanoparticles supported on nanoporous materials.

The present work represents the first use to our knowledge of exposed, nearly monodispersed Fe_2O_3 nanoparticles for PECVD growth of SWNTs. The Fe_2O_3 nanoparticles synthesized by using a fourth-generation, amine-terminated poly(amidoamine) (PAMAM) dendrimer (G4-NH_2) as a "nanotemplate" are highly susceptible to sintering and aggregation in the PECVD growth environment. In an effort to address this problem, favorable reaction conditions that enhance the stabilization of Fe nanoparticles in the PECVD reactor have been identified. These conditions, identified through the study of key parameters closely related to the catalyst, such as in situ annealing of catalyst in different atmospheres (H_2, N_2, Ar, and vacuum), catalyst−substrate interaction, and H_2 prereduction, have enabled the growth of high-quality SWNTs. CNTs grown by PECVD are usually plagued by the presence of amorphous carbon. The use of a positive dc bias voltage (+200 V) to eliminate amorphous carbon, while enhancing vertical alignment and graphitization of SWNTs, has also been demonstrated.

Experimental Section

Materials. An amine-terminated fourth-generation poly(amidoamine) (PAMAM) dendrimer having an ethylenediamine core (G4-NH_2) was purchased as a 10% methanol solution from Aldrich. The use of an amine-terminated dendrimer has an advantage in heterogeneous catalysis as it provides a reactive handle for linking the nanocomposite to surfaces.[12] $FeCl_3 \cdot 6H_2O$ was also purchased from Aldrich. Sapphire and SiO_2 (1 μ)-coated Si substrates were purchased from Saint Gobain and University Wafers, respectively. Porous anodic alumina (PAA) substrates were fabricated by a two-step anodization of a 1 μm Al film deposited on sapphire (with a 200 nm SiO_2 buffer layer). Anodization at 40 V in 0.3 M oxalic acid at 4 °C yielded a PAA film with ~40 nm diameter pores and an interpore spacing of ~100 nm. The Al films, the SiO_2 films on sapphire, and the 30 nm of Ti layer on silicon were deposited by e-beam evaporation.

Synthesis of Dendrimer-Templated Fe_2O_3 Nanoparticles. The Fe^{3+}/G4-NH_2 composite was synthesized according to a recipe described by Fahlman et al.[23] The G4-NH_2 dendrimer (0.4156 g, 0.12 mmol) and $FeCl_3 \cdot 6H_2O$ (0.5123 g, 1.89 mmol) were separately dissolved in 20 mL of deionized water and stirred for 10 min. Both solutions were combined and stirred vigorously for 4 h resulting in the formation of dendrimer-stabilized Fe^{3+} nanocomposite. Before dip coating, the substrates were washed several times with distilled water and ethanol, and then dried under a stream of N_2 gas. The composite was immobilized on the different substrates (SiO_2/Si, Ti/Si, sapphire, and PAA) by dip coating for 10 s, rinsing with deionized water to remove weakly bound particles, and drying in N_2. The immobilized Fe^{3+}/G4-NH_2 was calcined to remove the organic dendrimer, leaving behind nearly monodispersed Fe_2O_3 nanoparticles. The calcination process involved heating the immobilized Fe^{3+}/G4-NH_2 from room temperature to 550 °C at a rate of 30 deg/min in flowing air (500 sccm) and then maintaining the temperature at 550 °C for 5 min.

In this work, the amine groups on the periphery of the G4-NH_2 were not modified or protonated to favor the selective complexation of Fe^{3+} species with the interior tertiary amine groups of the G4-NH_2. The Fe nanoparticles have therefore been templated or stabilized via interdendritic encapsulation, which involves the preferential coordination of metal ions with the peripheral groups of the dendrimer.[12,23]

Growth of CNTs. The calcined catalyst (Fe_2O_3 nanoparticles) supported on SiO_2/Si, Ti/Si, sapphire, and PAA were used as templates for the growth of SWNTs by PECVD. Most reaction conditions employed were determined from a previous optimization study for SWNT growth over Mo/Co catalyst supported on nanoporous MgO.[22] A detailed description of the PECVD system and growth procedure is also reported therein. In brief, a typical growth process involved the introduction of the catalyst, which was placed on a 2-in. diameter molybdenum puck in the PECVD chamber. The puck facilitated the concentration of the plasma directly above the catalyst. The PECVD chamber was evacuated to a pressure of 0.5 Torr with an external mechanical pump. The chamber was thereafter purged with either H_2 (4.5 grade from Praxair), Ar, or N_2 for 5 min depending on the annealing environment that was being studied. However, prior to annealing the catalyst in a vacuum, the chamber was purged with N_2. Induction substrate heating supplied by a 3.5 kW RF source acting on a graphite susceptor upon which the Mo puck was placed was applied to heat the chamber to the reaction temperature (900 °C) in the different atmospheres (vacuum, H_2, N_2, and Ar). At reaction temperature, the chamber was evacuated and pressurized to 10 Torr, using 50 sccm of H_2. The H_2 plasma was ignited by using a power of 200 W, and 5 sccm of CH_4 (ultrahigh purity from Praxair) was fed into the chamber under these conditions for 20 min. At the end of each run, the chamber was evacuated and then allowed to cool to room temperature. The effect of H_2 prereduction of the catalyst on the growth of SWNTs was studied by exposing the catalysts to a flow of H_2 (50 sccm) at different temperatures and durations while annealing in N_2 atmosphere.

Characterization of Catalytic Template and CNTs. Immobilized catalytic nanoparticles were characterized with use of a Veeco DI Dimension 3100 AFM operating in the tapping mode. For this purpose, the Fe^{3+}/G4-NH_2 stock solution was diluted 50 times and cleaned mica substrates were immersed in the solution for 10 s, removed, rinsed with deionized water, and dried in air. The sample was also calcined in air as described previously. The as-synthesized carbon products were characterized with an Hitachi S-4800 field emission gun scanning electron microscope (FESEM) operated at 5 kV. Raman spectroscopic measurements of the products were also performed on a Renishaw Raman imaging microscope with a 785 nm (1.58 eV) diode laser as the excitation source. Each spectrum obtained was an average of three or four spectra acquired from multiple spots on the sample.

Results and Discussion

Characterization of Fe−Dendrimer Composites. Parts a and b of Figure 1 show an AFM image and the corresponding topographic height profile of nanoparticles formed on mica after immersing in pure $FeCl_3 \cdot 6H_2O$ solution (without PAMAM dendrimer). The mean size of the adsorbed Fe species was ~9.3 nm with nanoparticles showing a wide distribution in the range of 4−19 nm. As shown in Figure 1c,d, the use of a G4-NH_2 dendrimer to template and stabilize Fe^{3+} species of the same concentration as used in the control (Figures 1a,b) resulted

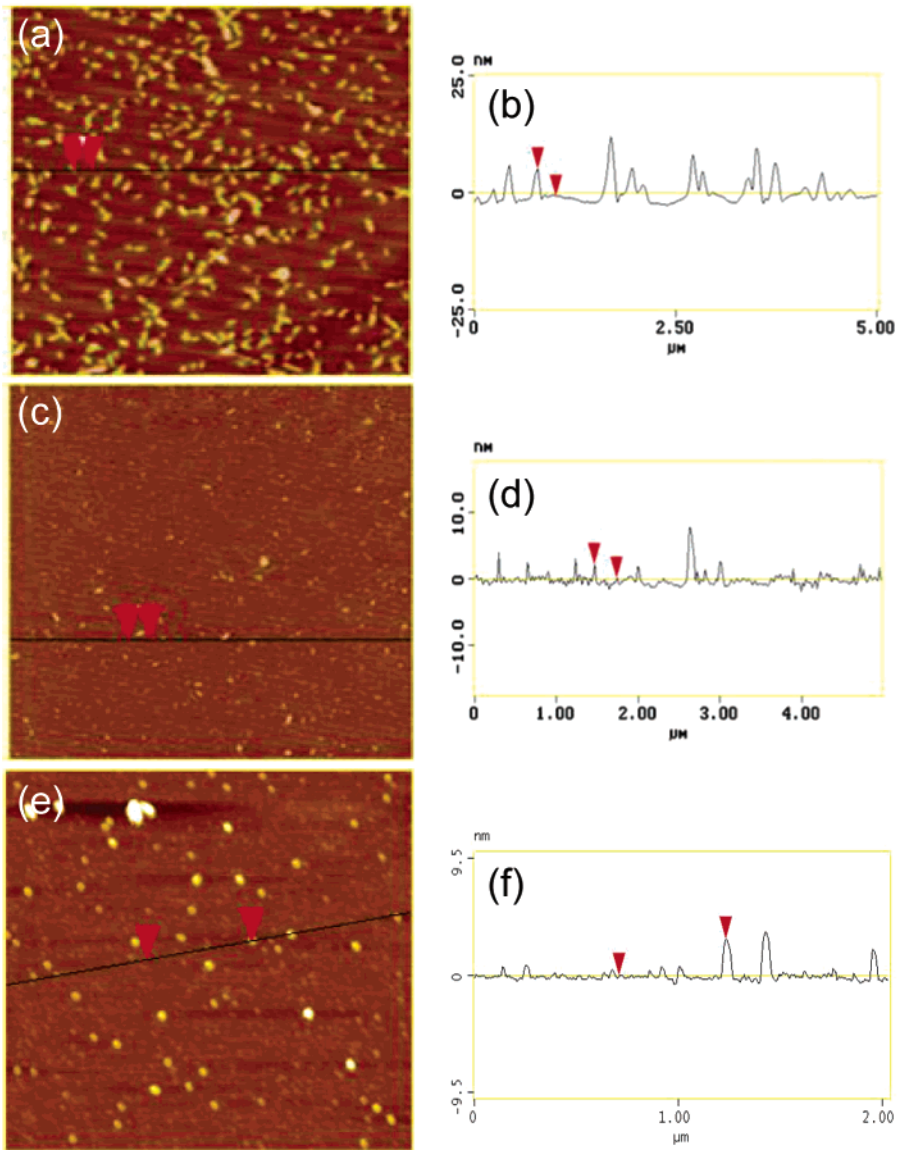

Figure 1. AFM images and topographic height profiles of adsorbed (a, b) Fe^{3+} species without G4-NH_2 dendrimers, (c, d) Fe^{3+}/G4-NH_2 nanocomposites, and (e, f) Fe_2O_3 nanoparticles obtained after calcination of (c) on mica substrates.

in smaller nanoparticles with a mean size of ~1.29 nm and a narrower distribution in the range of <1 to 3 nm. A small percentage of nanoparticles of larger sizes, between 5 and 7 nm, were also observed. After calcination of the mica-supported Fe^{3+}/G4-NH_2 composite at 550 °C for 5 min in air, the size of the nanoparticles increased to a mean size of ~3.2 nm as shown in Figures 1e,f. Upon calcination of the mica-supported Fe^{3+} sample (without a dendrimer), we observed a mean size of ~20 nm (result not shown for the sake of brevity). Figure 2 shows the particle-size histograms, which have been adapted from Figure 1. The narrow particle size distribution shown by the dendrimer-templated Fe nanoparticles clearly demonstrates the efficacy of the PAMAM dendrimer in enhancing monodispersity.

The apparent height from AFM topographic profiles obtained by tapping-mode AFM is normally affected by several environmental factors.[24] Therefore, the mean nanoparticle sizes presented here are not absolute. In addition, the catalyst solution dip coated on mica substrates was diluted 50-fold. However, the relative difference in the mean particle size of the dendrimer-templated nanoparticles and the nanoparticles synthesized in the absence of the dendrimer is meaningful.

The use of a G4-NH_2 to template and stabilize Fe^{3+} species yields nearly monodispersed nanoparticles with a mean size of ~1.3 nm. The increase in nanoparticle size observed upon removal of the G4-NH_2 by calcination is a common problem associated with the use of dendrimer-encapsulated or stabilized metal nanoparticles in heterogeneous catalysis.[12] Work is in progress to investigate effective methods of removing the dendrimer without compromising the monodispersity of the metal nanoparticles. The AFM images of Fe-stabilized dendrimer (Figure 1c) and Fe_2O_3 nanoparticles (Figure 1e) reveal well-dispersed nanoparticles on the substrate after 10 s of dip coating in the composite solution. High dispersity of catalyst nanoparticles correlates with high catalytic activity and narrow diameter distribution of SWNTs produced during growth by CVD.[10]

Previous reports suggest that the size limit of metal nanoparticles that can nucleate SWNTs during CVD growth is 5 to 6 nm[6a] or 4 to 8 nm.[6b] In this work with PECVD, the increase in nanoparticle size that occurs upon calcination of the immobilized Fe^{3+}/G4-NH_2 composite was not an impediment to SWNT growth. We observed that the substrate temperature is at least as important as the catalyst particle size in defining the

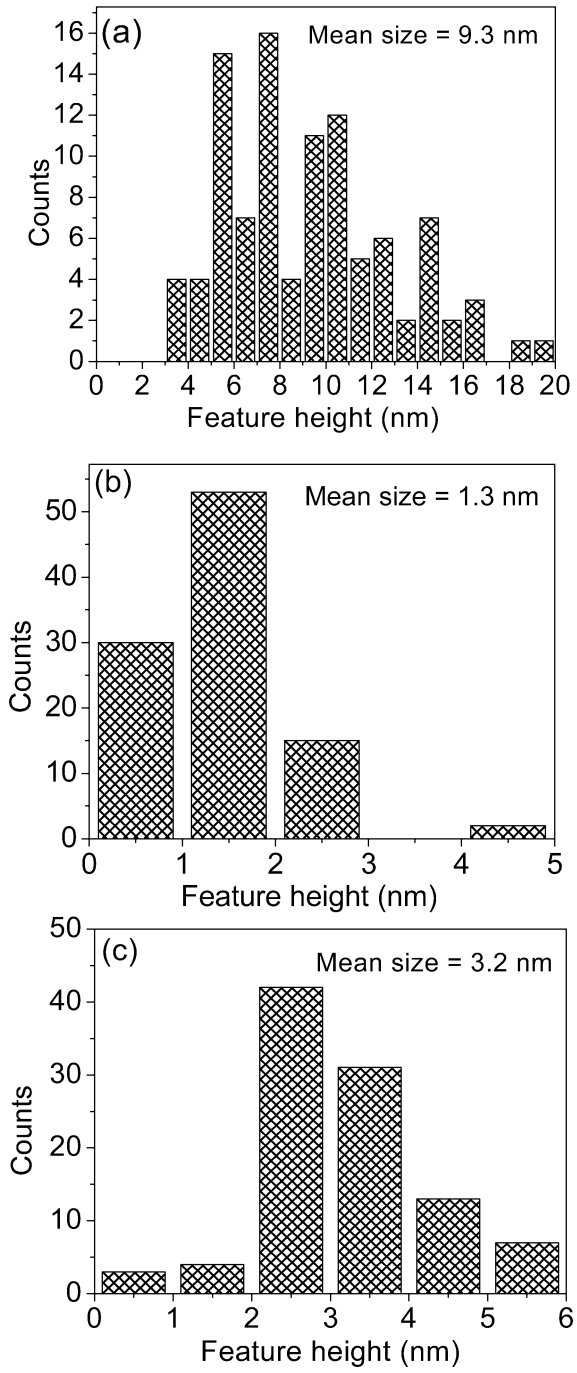

Figure 2. Particle-size histograms of (a) Fe^{3+} species without G4-NH_2 dendrimers, (b) Fe^{3+}/G4-NH_2 nanocomposites, and (c) Fe_2O_3 nanoparticles obtained after calcination of (b) on mica substrates; adapted from Figure 1.

process conditions for SWNT growth. As the catalyst particle size increases, the minimum temperature necessary for SWNT growth also increases. The minimum temperature that resulted in SWNT growth with use of the catalyst nanoparticles produced in the present study was 900 °C, while lower temperatures produced a predominance of MWNTs. The report of Homma et al.[25] gives credence to this result, as they reported that Fe particles with a size range of 10−30 nm show SWNT selectivity at 900−950 °C by CVD, whereas a minimum temperature of 800 °C was necessary for MWNT growth.

Effect of Annealing Ambient. During the ramping of the reactor temperature, metal nanoparticles become more mobile, resulting in a coarsening and an increase in the particle size distribution. Nanoparticle mobility depends on several factors, including the annealing environment and the nature of the metal−support interaction. The difficulty associated with the growth of SWNT via PECVD with Fe catalysts may in part be due to the severe aggregation that occurs during annealing or the lack of stabilization of catalyst nanoparticles. In an effort to address this problem, a study involving the annealing of Fe catalyst in different environments (N_2, Ar, H_2, and vacuum) prior to CNT growth was performed to identify favorable annealing environment(s) that enhance stabilization of Fe catalyst and, consequently, increased SWNT selectivity and quality.

Raman spectroscopic measurements were carried out on all the carbon products obtained after growth. Typical Raman spectra of CNTs are characterized by four Raman bands that are strongly resonance enhanced.[26] The bands are the G-band, the D-band, the Breit−Wigner−Fano (BWF) line, and the radial breathing mode (RBM). The G-band near 1590 cm^{-1} originates from the in-plane stretching mode of the graphene sheets. The D-band occurs near 1310 cm^{-1} and is associated with the presence of amorphous carbon and defects in graphene sheets. The BWF line occurring near 1500 cm^{-1} and typically as a shoulder of the G-band is considered to be a characteristic Raman mode of metallic SWNTs. The presence of the RBM modes in the lower frequency region is strong evidence that the carbon material contains SWNTs. From the RBM frequency (ω_{RBM}), it is possible to determine the diameter of the SWNT by using the relation for SWNT bundles ω_{RBM} (cm^{-1}) = 12.5 + 223.5/d (nm).[27] The integrated intensity of the G-band (I_G) relative to the D-band (I_D) is used in this work for qualitative evaluation of CNT quality. The use of the I_G/I_D ratio in characterizing quality does have certain limitations, as these bands are sensitive to effects such as doping.[28] For CVD-grown CNTs, a I_G/I_D band ratio of 4 is considered as a benchmark for high-quality products.[29]

The Raman spectra of CNTs grown from SiO_2/Si-supported catalysts annealed in different atmospheres are presented in Figure 3. The typical spectral features (G- and D-bands) are observed in all the Raman spectra, indicating that CNTs were produced. The spectra of CNTs grown from catalysts annealed in N_2, Ar, and vacuum showed RBM modes in the low-frequency region confirming the presence of SWNTs in these samples. SWNTs grown from catalysts annealed in Ar and vacuum showed several RBM peaks in the range of 180−250 cm^{-1} while SWNTs grown from catalysts annealed in N_2 showed an intense RBM peak at 270 cm^{-1} with a small peak at 235 cm^{-1}. The former peaks in the range of 180−250 cm^{-1} correspond to tube diameters of 0.94−1.35 nm. The latter peaks at 270 and 235 cm^{-1} correspond to tube diameters of 0.87 and 1.00 nm. Therefore, SWNTs grown from Fe catalyst annealed in Ar may have a wide distribution of diameters. We also note that the presence of a dominant RBM peak as observed for catalysts annealed in N_2 does not necessarily indicate a narrow distribution of tube diameters. Because of the strong resonant enhancement effect,[26] whereby the RBM peaks vary with the laser excitation energy, such a conclusion cannot be reached with the use of a single laser excitation energy. Catalysts annealed in a vacuum and H_2 produced relatively low amounts of CNTs as indicated by the weak Raman signals. It is also clear from Figure 3 that annealing Fe catalysts in Ar or N_2 atmospheres increases CNT selectivity as observed by the strong intensity of the G-band.

Figure 4 shows representative FESEM images of CNTs grown from Fe catalysts supported on SiO_2/Si and annealed in N_2, Ar, vacuum, and H_2 atmospheres. Catalyst nanoparticles annealed

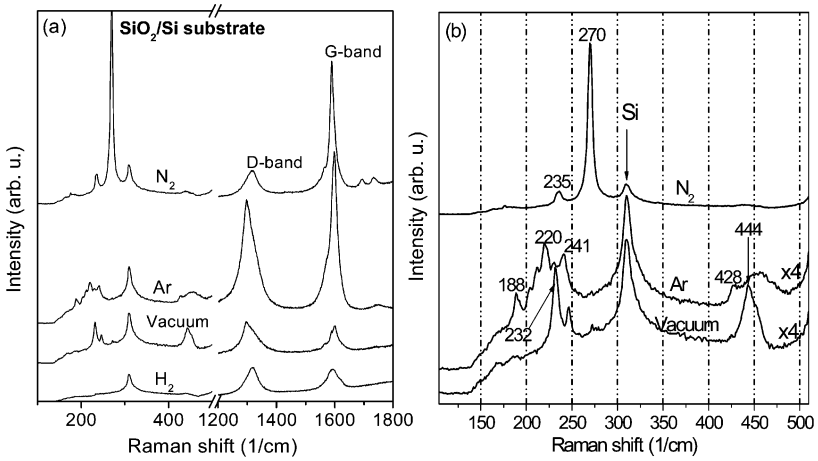

Figure 3. Raman spectra of CNTs grown from SiO_2/Si-supported catalysts annealed in different atmospheres (a) and the low-frequency region (b).

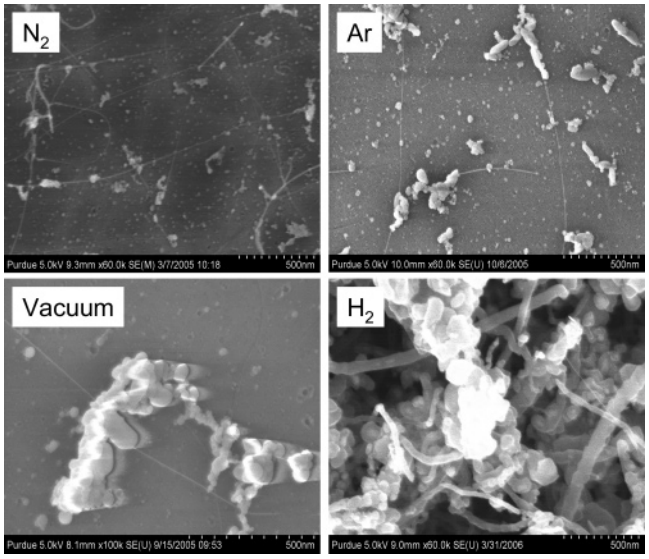

Figure 4. FESEM images of CNTs grown from SiO_2/Si-supported catalysts annealed in N_2, Ar, vacuum, and H_2 atmospheres.

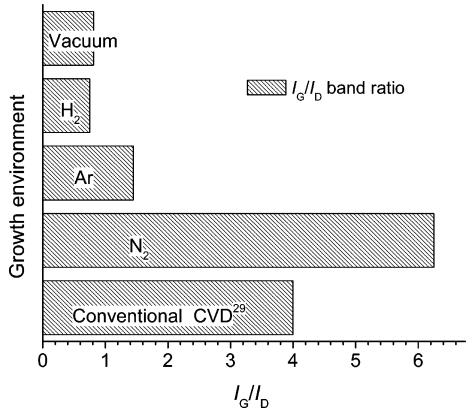

Figure 5. The quality of CNTs grown from SiO_2/Si-supported catalysts annealed in the different atmospheres. The quality of CNTs has been expressed in terms of I_G/I_D band ratio.

in a N_2 atmosphere produced principally SWNTs and few MWNTs. The SWNTs were straight and usually isolated, although bundles were occasionally observed. As a common feature for all growth runs, the respective FESEM images revealed that not all the nanoparticles on the substrate nucleated the growth of CNTs. The yield of CNTs is low in comparison to the total number of nanoparticles on the substrate.

For catalysts annealed in N_2, the surface was comparatively free of large metal particles, suggesting that the stabilization of Fe nanoparticles is enhanced under this condition. The quality of CNTs grown from catalysts annealed in the different atmospheres is presented in Figure 5. CNTs grown from catalysts annealed in N_2 showed the highest quality, with an I_G/I_D ratio of 6.2. To rationalize the stabilization of Fe nanoparticles annealed in N_2 environment, further in situ spectroscopic studies should be carried out. However, based on Ostwald ripening, the melting point of Fe−N is well above that of Fe. Fe−N species would therefore exhibit higher stability than Fe during PECVD growth of CNTs.

Catalysts annealed in Ar produced mixtures of SWNTs and MWNTs (Figure 4). The Raman result (Figure 3) revealed several RBM peaks, suggesting that Fe catalyst annealed in Ar may grow SWNTs with a wide diameter distribution. In addition, the quality of these SWNTs is relatively lower than that of SWNTs grown from catalyst annealed in N_2. As presented in Figure 5, the I_G/I_D ratio for this sample is 1.45, which is much lower than the benchmark for CVD grown SWNTs. The relatively low stabilization of Fe nanoparticles annealed in Ar atmosphere could be playing a role in these results.

We observed that early H_2 reduction of Fe_2O_3 to Fe^0 during annealing favors aggregation of metal particles because of their increased mobility under a reducing environment. As shown in Figure 4, catalysts annealed in H_2 produced large metallic particles (>20 nm) and were generally more selective for MWNT growth with high amounts of amorphous carbon. Nanotubes grown under this condition showed the lowest quality (I_G/I_D ratio of 0.75) as shown in Figure 5. The absence of RBM peaks in the Raman spectrum of this sample suggests that no SWNTs were grown. The large metallic particles formed are apparently above the upper size limit of particles selective for SWNT growth at this temperature and reaction condition.

Annealing Fe catalysts in a vacuum resulted in the formation of a low density of large metallic particles (Figure 4). The nanotubes grown were principally SWNTs. Sintering of catalytic sites may have occurred because fewer particles in comparison to previous cases nucleated the growth of SWNTs. The SWNT density was low as shown in Figure 4d and this observation is supported by the low intensities of their Raman peaks (Figure 3). The quality of SWNTs produced was low as evidenced by an I_G/I_D band ratio of 0.81 presented in Figure 5. On the basis of the frequency of the RBM peaks at 232 and 246 cm^{-1}, the corresponding diameters of SWNTs grown were 1.02, and 0.96 nm.

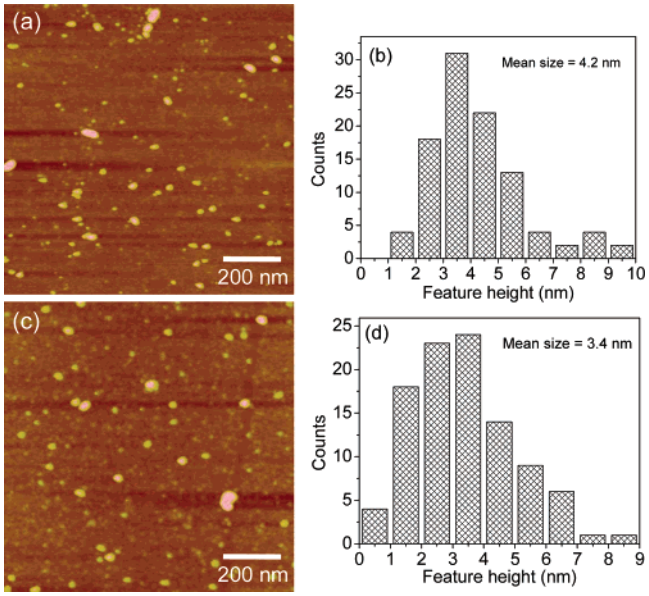

Figure 6. AFM images and their corresponding particle-size histograms of Fe_2O_3 nanoparticles after annealing in Ar (a, b) and N_2 (c, d) atmospheres.

An important conclusion drawn from this study is that annealing SiO_2-supported Fe_2O_3 nanoparticles in an N_2 atmosphere enhances their stabilization during nanotube growth in the PECVD, resulting in increased SWNT selectivity and quality. The effect of annealing ambient (N_2 and Ar) on the size distribution of calcined Fe-templated nanoparticles supported on mica was studied by using an AFM, and the results are presented in Figure 6. From the particle size histograms (Figure 6b,d), it is clear that annealing in an N_2 atmosphere showed slight stabilization of Fe_2O_3 nanoparticles. In comparison to the native sample (Figures 1e and 2c) and the sample annealed in Ar atmosphere (Figure 6a,b), there is a significant increase in the number of particles less than 2 nm in size after annealing in an N_2 atmosphere. Also, 68% of the particles counted were smaller than 4 nm as opposed to 53% for particles annealed in Ar atmosphere.

The low SWNT density observed may be due to the relatively large size of Fe_2O_3 particles obtained after calcination. Efficient removal of the dendrimer without compromising the near monodispersity may increase SWNT density. The growth of SWNTs on SiO_2-coated substrates has been a major challenge because of the weak interaction between Fe particles and SiO_2 in comparison to Al_2O_3.[30] In addition, the H_2 plasma is capable of reducing the SiO_2 film on the substrate, which could result in the formation of a silicide, a well-known catalyst poison. The present approach is capable of improving the PECVD synthesis of SWNTs from exposed Fe nanoparticles.

Note that a control growth experiment was carried out with an Fe_2O_3 catalyst synthesized from pure $FeCl_3 \cdot 6H_2O$ solution without the dendrimer (results not shown). The catalyst was annealed in an N_2 atmosphere during nanotube growth, and the products were mainly thick MWNTs with large amounts of amorphous carbon ($I_G/I_D < 0.1$). We also note that SWNTs could be grown from the immobilized Fe^{3+}/G4-NH_2 composite that was not subjected to the calcination step. However, we found this step to be necessary in order to maintain surface cleanliness.

Effect of Catalyst Support Material. The catalyst−substrate interaction is a key factor during the CVD growth of SWNTs and has been well studied. Among the three substrates used by Zheng et al.[31] for CVD growth of SWNTs using H_2 and CO

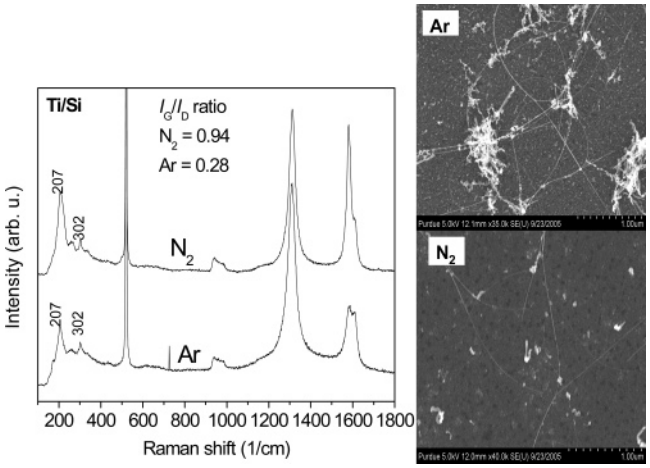

Figure 7. Raman spectra of SWNTs grown from Si/Ti-supported catalyst and their corresponding FESEM images of SWNTs grown from catalyst annealed in Ar and N_2 atmospheres.

mixtures, SiO_2/Si-supported Fe catalysts showed the highest yield of SWNTs, while Al_2O_3-supported Fe catalyst showed the lowest yield. On the other hand, Su et al.[32] observed a low yield of SWNTs on Si- and SiO_2/Si-supported Fe−Mo catalyst during CH_4 CVD, and the highest SWNT yield was observed for Fe−Mo supported on a Al_2O_3 monolayer. We have investigated the effect of the metal−support interaction on SWNT growth from Fe_2O_3 nanoparticles supported on Ti/Si, sapphire, and PAA and annealed in N_2 and Ar environments.

Figure 7 shows Raman spectra and representative FESEM images of SWNT bundles grown from Fe catalyst supported on Ti/Si. From the Raman spectra, RBM peaks at 207 and 302 cm^{-1} were identified, corresponding to SWNT diameters of 1.1 and 0.78 nm, respectively. FESEM studies revealed that mixtures of SWNTs and MWNTs were produced for Ti/Si-supported catalysts. However, a higher selectivity to SWNTs was observed for catalysts annealed in N_2. SWNTs grown from catalyst supported on Ti/Si were of relatively low quality, as evidenced by very low I_G/I_D band ratios (<1). Consistent with previous observations, catalysts annealed in N_2 produced SWNTs with a slightly higher quality, and the absence of large Fe particles on the surface (Figure 7) suggests that N_2-annealed catalyst nanoparticles were relatively stable.

For catalysts supported on Al_2O_3 (sapphire and PAA), the results of Raman spectra shown in Figure 8 indicate that SWNTs grow efficiently on these substrates with very little amorphous carbon deposition. The I_G/I_D band ratios are as high as ~10, which is more than two times higher than the benchmark for CVD-grown CNTs. Al_2O_3 is a known texture promoter of Fe, as its presence enhances stabilization, porosity, and the surface area of Fe catalyst.[33] The strong interaction that exists between Al_2O_3 and Fe nanoparticles decreases nanoparticle aggregation and coalescence, thereby maintaining Fe nanoparticles in a size range that is selective for SWNT growth. Most SWNTs observed for both sapphire- and PAA-supported catalysts were bundles consisting of tens or hundreds of individual SWNTs that were highly branched. It is possible that individual SWNTs were present, but the limited resolution of the FESEM makes it difficult to image them. Consistent with SiO_2/Si- and Ti/Si-supported catalysts, catalysts on Al_2O_3 were also affected (albeit mildly for PAA) by the annealing environment. The I_G/I_D band ratio for SWNTs grown from catalysts annealed in N_2 was 9.3 compared to a I_G/I_D band ratio of 4.8 for SWNTs grown from catalysts annealed in Ar. However, we consistently observed multiple RBM peaks for SWNTs grown from catalysts annealed

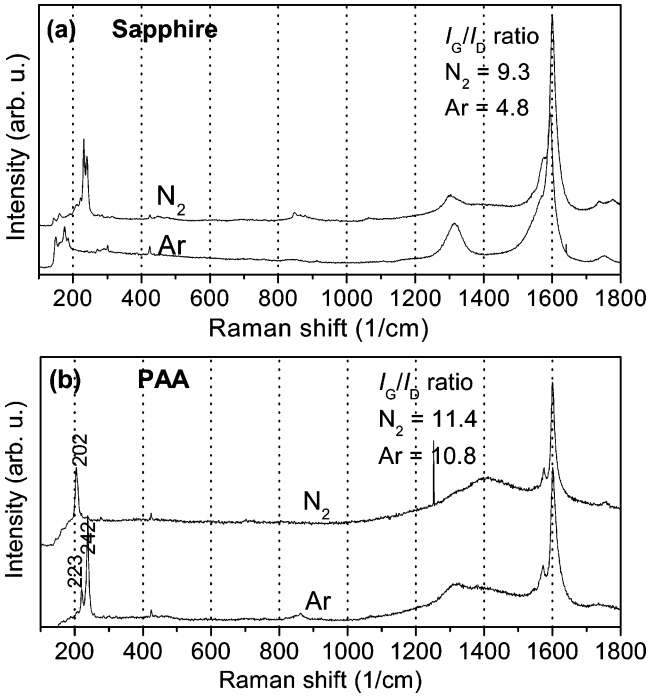

Figure 8. Raman spectra of SWNTs grown from catalyst supported on sapphire (a) and PAA (b) annealed in N_2 or Ar.

in Ar, while SWNTs grown from catalysts annealed in N_2 showed fewer peaks, and a single peak in the case of PAA-supported catalyst (Figure 8b). The BWF line, a characteristic Raman mode of metallic SWNTs, is present in the Raman spectra of SWNTs grown on sapphire and PAA. For the most part, we observed the same behavior for PAA- and sapphire-supported catalysts. However, a major difference was observed in their Raman spectra as SWNTs grown on PAA-supported catalysts showed broadened D-bands. The reason for this behavior is still under investigation. The different results obtained for SiO_2/Si- and Al_2O_3-supported catalyst may be due to the different chemical and morphological changes induced in the catalyst because of the catalyst−substrate interaction.[30]

Effects of H_2 Prereduction. Most mechanisms[4a,34,35] proposed to date for the growth of SWNTs have identified a reduced form of metallic nanoparticles (typically, those of Fe, Ni, and Co) as the active species that nucleates nanotube growth. This proposition suggests that careful optimization of the H_2 prereduction treatment can improve catalytic activity and consequently SWNT selectivity and quality. For most catalytic systems used for SWNT growth, a reduction step in a temperature range of 500−700 °C is critical to catalytic activity and SWNT selectivity.[4a,35] The present work involving SWNT growth via CH_4 decomposition in the PECVD reactor has revealed slightly different results.

We have investigated the effects of catalyst prereduction at different temperatures in the range of 500−900 °C on SWNT growth. Representative results for SiO_2/Si- and sapphire-supported catalysts prereduced at the reduction temperature of Fe (∼500 °C)[16] and the reaction temperature (900 °C) are presented in Figures 10 and 11. From several growth runs, it was established that a short prereduction time of ∼5 min was beneficial for high SWNT selectivity with comparatively low amorphous carbon content. Prolonged prereduction (>5 min) resulted in the formation of mainly MWNTs, accompanied by high amounts of amorphous carbon.

The Raman spectra of nanotubes grown on SiO_2/Si- and sapphire-supported substrates are presented in Figure 10, parts

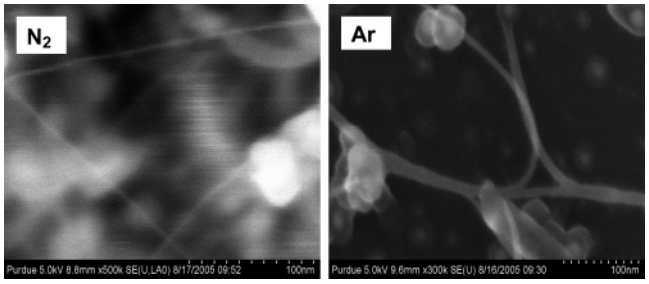

Figure 9. FESEM images of SWNT bundles grown on sapphire-supported catalyst annealed in N_2 and Ar.

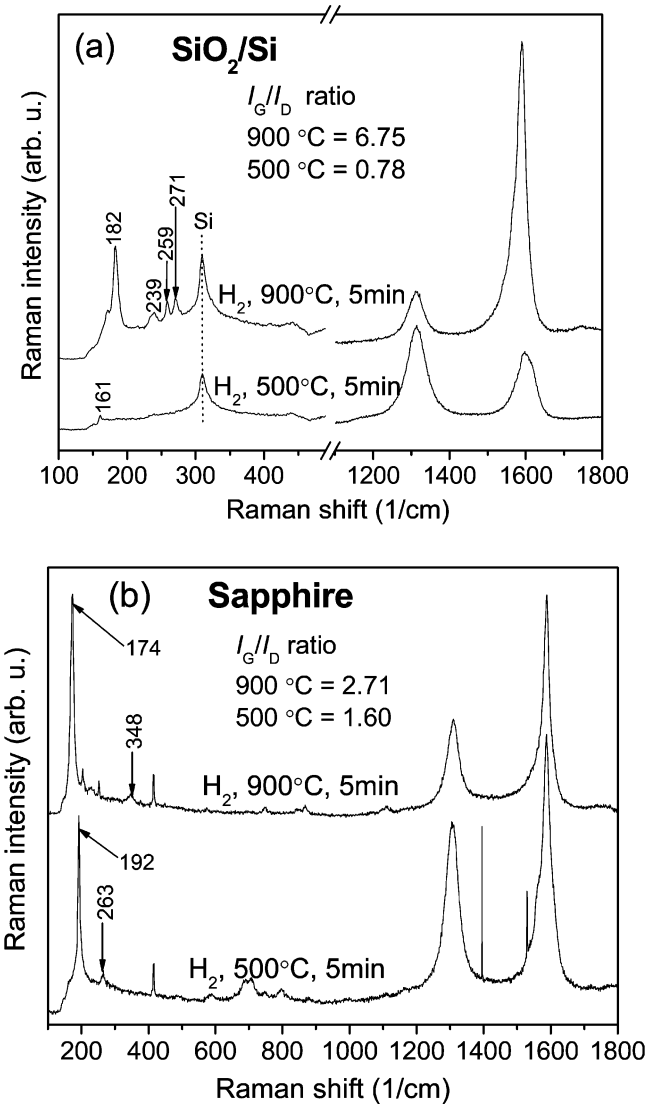

Figure 10. Raman spectra of SWNTs grown from SiO_2/Si-supported (a) and sapphire-supported (b) catalysts.

a and b, respectively. These results, especially for SiO_2/Si-supported catalysts, indicate that prereduction at 500 °C is detrimental to SWNT selectivity and quality. The RBM peak observed near 160 cm^{-1} in the Raman spectrum is inconspicuous; FESEM images (Figure 11a) confirmed the low SWNT selectivity. However, it is possible that other SWNT diameters may be present but not detected by Raman spectroscopy because of the resonance enhancement phenomenon.[26] The quality of nanotubes grown after this pretreatment was poor, evidenced by the low I_G/I_D band ratio (0.78). However, a distinct variation in the SWNT selectivity and quality was observed for catalysts prereduced at 900 °C. SWNTs grown after prereduction at 900

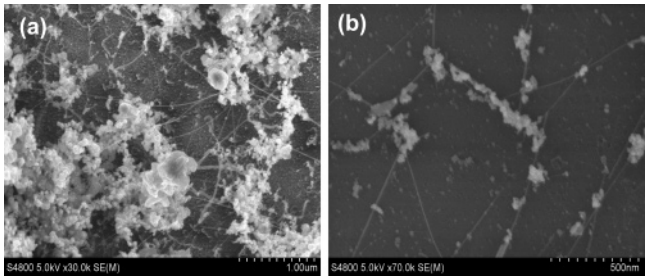

Figure 11. FESEM images of CNTs grown from SiO_2/Si-supported catalyst prereduced for 5 min at 500 (a) and 900 °C (b).

°C showed a well-defined RBM peak near 182 cm^{-1} with smaller peaks at 239, 259, and 271 cm^{-1}, corresponding to SWNT diameters of 1.3, 0.99, 0.91, and 0.87 nm, respectively. The Raman results (Figure 10a) indicate that prereducing the catalyst at 900 °C for 5 min increases SWNT selectivity. The existence of several strong RBM peaks in the Raman spectrum of this sample is attributed to effect of prereduction because these peaks were not observed for SWNTs grown from the unreduced catalyst. Even though prereduction at the reaction temperature increases SWNT selectivity, it also results in a wider distribution of SWNT diameters. The high value of the I_G/I_D band ratio (6.75) observed for catalysts prereduced at 900 °C indicates that the quality is much improved. In addition, the I_G/I_D band ratio is slightly higher than that obtained for growth from unreduced catalyst (I_G/I_D band ratio of 6.2), suggesting that this form of pretreatment is highly desirable for the SiO_2/Si-supported catalyst.

The respective FESEM images of nanotubes grown from catalysts prereduced at 500 and 900 °C are presented in Figure 11, parts a and b, respectively. Consistent with the Raman results, the nanotubes grown from the catalyst prereduced at 500 °C were mixtures of MWNTs and SWNT bundles, while those grown from catalyst prereduced at 900 °C were mainly SWNT bundles. Prereduction at 500 °C results in the formation of several large Fe particles that were present over much of the substrate.

Interestingly, for sapphire-supported catalysts, SWNT selectivity was not significantly affected by prereduction at 500 °C, probably because of the high stabilization of Fe particles that occurs on Al_2O_3. Results of Raman spectroscopy shown in Figure 10b indicate that catalysts prereduced at 500 and 900 °C are both selective for SWNTs, evidenced by the presence of strong RBM modes at 192 and 174 cm^{-1}, respectively. These RBM modes correspond to SWNT diameters of 1.2 and 1.4 nm. Despite their high SWNT selectivity, the amount of amorphous carbon produced was comparatively high, as their respective I_G/I_D band ratios (<4) suggest. This high catalytic activity of sapphire-supported catalyst may be due to the formation of $FeAl_2O_4$ on the surface upon reduction, which favors the growth of an adlayer of the most active form of Fe-(111) surface.[33] As observed previously for SiO_2/Si-supported catalysts, the prereduction of sapphire-supported catalysts at 900 °C also resulted in SWNTs with a higher I_G/I_D band ratio (2.71).

Effects of dc Bias Voltage. High-quality SWNTs were effectively grown on sapphire-supported catalysts under either positive or negative dc bias voltage of 200 V. Their Raman spectra and corresponding representative cross sectional FESEM images are presented in Figure 12. Using these characterization tools, we found no evidence of amorphous carbon or MWNTs for SWNTs grown under positive dc bias voltage. The result unambiguously demonstrates that the growth of SWNTs under positive dc bias voltage (200 V) is a suitable condition for the

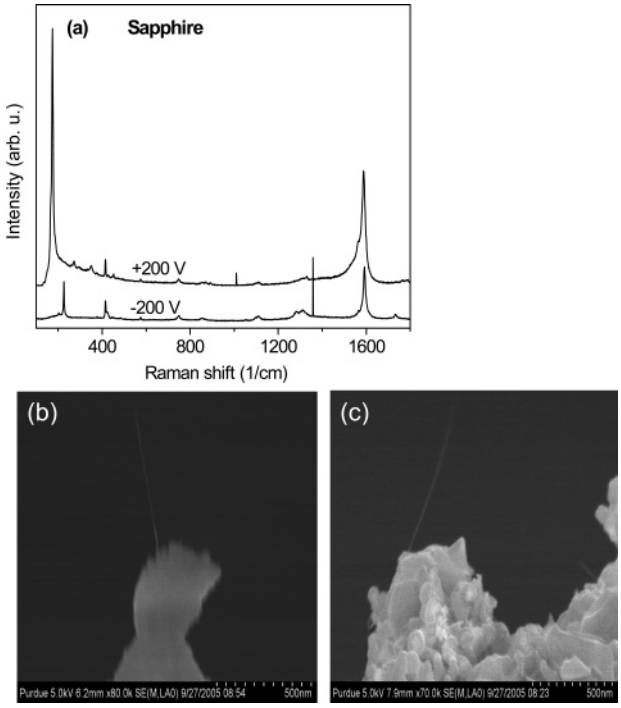

Figure 12. Raman spectra of SWNTs grown from sapphire-supported catalyst under positive and negative dc bias voltage (a); FESEM images of SWNTs grown under (b) −200 and (c) +200 V.

selective growth of high-quality SWNTs free of amorphous carbon. The intense RBM peaks, the narrow G-band, and the absence of the D-band for SWNTs grown under positive bias are strong indications that the SWNTs are well graphitized and of high quality. Under positive substrate bias, electrons will tend to be more attracted to the substrate, while positive hydrogen ions are repelled.

The few vertically aligned SWNT bundles observed in the FESEM images presented in Figure 12b,c do not necessarily suggest poor SWNT yield because at the highest resolution of the FESEM, it is difficult to image individual SWNTs in different focal planes. The FESEM resolution is well adapted for the characterization of MWNTs; for these samples, no MWNTs were observed.

Conclusions

We have presented the first results of the growth of SWNTs by PECVD using dendrimer-templated and stabilized, nearly monodispersed Fe_2O_3 nanoparticles. The reaction conditions that favor stabilization of these exposed Fe_2O_3 nanoparticles in the unique growth environment of the PECVD, resulting in higher SWNT selectivity and quality, have been identified. These studies show that SWNT selectivity and quality are enhanced by annealing SiO_2/Si-, Ti/Si-, and sapphire-supported Fe catalyst in an N_2 atmosphere. Prereduction of the catalyst at 900 °C for 5 min increased SWNT selectivity and quality for SiO_2/Si-supported catalyst. High SWNT selectivity was observed for both reduced and unreduced catalyst supported on Al_2O_3, albeit of lower quality for the former. The application of a positive dc bias voltage of 200 V was very effective in eliminating carbon impurities, while enhancing graphitization, SWNT selectivity, and vertical alignment.

Acknowledgment. This research is supported by the NASA-Purdue Institute for Nanoelectronics and Computing and the Birck Nanotechnology Center. Thanks are due to Prof. Lynne

Taylor and Dr. Alan Gift for access to the Raman instrument, and to Drs. Xi Zhang and Shamim Mirza for AFM assistance.

References and Notes

(1) Iijima, S. *Nature* **1991**, *354*, 56.

(2) Dresselhaus, M. S.; Dresselhaus, G.; Eklund, P. C. *Science of Fullerenes and Carbon Nanotubes*; Academic Press: New York, 1996.

(3) (a) Dai, H. J.; Rinzler, A. G.; Nikolaev, P.; Thess, A.; Colbert, D. T.; Smalley, R. E. *Chem. Phys. Lett.* **1996**, *260*, 471. (b) Sinnott, S. B.; Andrews, R.; Qian, D.; Rao, A. M.; Mao, Z.; Dickey, E. C.; Derbyshire, F. *Chem. Phys. Lett.* **1999**, *315*, 25. (c) Cheung C. L.; Kurtz, A.; Park, H.; Lieber, C. M. *J. Phys. Chem. B* **2002**, *106*, 2429. (d) Ciuparu, D.; Chen, Y.; Lim, S.; Haller, G. L.; Pfefferle, L. *J. Phys. Chem. B* **2004**, *108*, 503.

(4) (a) Chen Y.; Ciuparu, D.; Lim, S.; Yang, Y.; Haller, G. L.; Pfefferle, L. *J. Catal.* **2004**, *225*, 453. (b) Ago, H.; Imamura, S.; Okazaki, T.; Saito, T.; Yumura, M.; Tsuji, M. *J. Phys. Chem. B* **2005**, *109*, 10035.

(5) Choi, H. C.; Kim, W.; Wang, D.; Dai, H. *J. Phys. Chem. B* **2002**, *106*, 12361.

(6) (a) Li, Y.; Kim, W.; Zhang, Y.; Rolandi, M.; Wang, D.; Dai, H. *J. Phys. Chem. B* **2001**, *105*, 11424. (b) Li, Y.; Liu, J.; Wang, Y.; Wang, Z. L. *Chem. Mater.* **2001**, *13*, 1008.

(7) Mizuno, K.; Hata, K.; Saito, T.; Ohshima, S.; Yumura, M.; Iijima, S. *J. Phys. Chem. B* **2005**, *109*, 2632.

(8) Ando, Y.; Zhao, X.; Sugai, T.; Kumar, M. *Mater. Today* **2004**, *7*, 22.

(9) Hornyak, G. L.; Grigorian, L.; Dillon, A. C.; Parilla, P. A.; Jones, K. M.; Heben, M. J. *J. Phys. Chem. B* **2002**, *106*, 2821.

(10) Cassel, A. M.; Raymakers, J. A.; Kong, J.; Dai, H. *J. Phys. Chem. B* **1999**, *103*, 6484.

(11) Peigney, A.; Coquay, P.; Flahaut, E.; Vandenberghe, R. E.; De Grave, E.; Laurent, C. *J. Phys. Chem. B* **2001**, *105*, 9699.

(12) Scott, R. W. J.; Wilson, O. M.; Crooks, R. M. *J. Phys. Chem. B* **2005**, *109*, 692.

(13) Li, Y.; Liu, J.; Wang, Y.; Wang, Z. L. *Chem. Mater*. **2001**, *13*, 1008.

(14) Park, S. J.; Kim, S.; Lee, S.; Khim, Z. G.; Char, K.; Hyeon, T. *J. Am. Chem. Soc.* **2000**, *122*, 8581.

(15) Ago, H.; Nakamura, K.; Uehara, N.; Tsuji, M. *J. Phys. Chem. B* **2004**, *108*, 18908.

(16) Amama, P. B.; Lim, S.; Ciuparu, D.; Yang, Y.; Pfefferle, L.; Haller, G. L. *J. Phys. Chem. B* **2005**, *109*, 2645.

(17) Mizuno, K.; Hata, K.; Saito, T.; Ohshima, S.; Yumura, M.; Iijima, S. *J. Phys. Chem. B* **2005**, *109*, 2632.

(18) Su, M.; Li, Y.; Maynor, B.; Buldum, A.; Lu, J. P.; Liu, J. *J. Phys. Chem. B* **2000**, *28*, 6505.

(19) Wang, X.; Yue, W.; He, M.; Liu, M.; Zhang, J.; Liu, Z. *Chem. Mater*. **2004**, *16*, 799.

(20) Melechko, A. V.; Merkulov, V. I.; McKnight, T. E.; Guillorn, M. A.; Klein, K. L.; Lowndes, D. H.; Simpson, M. L. *J. Appl. Phys.* **2005**, *97*, 041301.

(21) (a) Kato, T.; Jeong, G.; Hirata, T.; Hatakeyama, R.; Tohji, K.; Motomiya, K. *Chem. Phys. Lett.* **2003**, *381*, 422. (b) Kato, T.; Jeong, G.; Hirata, T.; Hatakeyama, R.; Tohji, K. *Jpn. J. Appl. Phys.* **2004**, *43*, L1278. (c) Li, Y.; Mann, D.; Rolandi, M.; Kim, W.; Ural, A.; Hung, S.; et al. *Nano Lett.* **2004**, *4*, 317. (d) Delzeit, L.; Nguyen, C. V.; Stevens, R. M.; Han, J.; Meyyappan, M. *Nanotechnology* **2002**, *13*, 280.

(22) Maschmann, M. R.; Amama, P. B.; Goyal, A.; Iqbal, Z.; Gat, R.; Fisher, T. S. *Carbon* **2006**, *44*, 10.

(23) Vohs, J. K.; Brege, J. J.; Raymond, J. E.; Brown, A. E.; Williams, G. L.; Fahlman, B. D. *J. Am. Chem. Soc*. **2004**, *126*, 9936.

(24) (a) Knoll, A.; Magerle, R.; Krausch, G. *Macromolecules* **2001**, *34*, 4159. (b) Brandsch, R.; Bar, G.; Whangbo, M.-H. *Langmuir* **1997**, *13*, 6349. (c) Su, M.; Zheng, B.; Liu, J. *Chem. Phys. Lett.* **2000**, *322*, 321.

(25) Homma, Y.; Yamashita, T.; Finnie, P.; Tomita, M.; Ogino, T. *Jpn. J. Appl. Phys.* **2002**, *41*, L89.

(26) Dresselhaus, M. S.; Eklund, P. C. *Adv. Phys.* **2000**, *49*, 705.

(27) Bachilo, S. M.; Strano, M. S.; Kittrell, C.; Hauge, R. H.; Smalley, R. E.; Weisman, R. B. *Science* **2002**, *298*, 2361.

(28) O'Connell, M. J.; Eibergen, E. E.; Doorn, S. K. *Nature Mater*. **2005**, *4*, 412.

(29) Okamoto, A.; Shinohara, H. *Carbon* **2005**, *43*, 431.

(30) Arcos, T.; Garnier, M. G.; Seo, J. W.; Oelhafen, P.; Thommen, V.; Mathys, D. *J. Phys. Chem. B* **2004**, *108*, 7728.

(31) Zheng, B.; Lu, C.; Gu, G.; Makarovski, A.; Finkelstein, G.; Liu, J. *Nano Lett.* **2002**, *2*, 895.

(32) Su, M.; Li, Y.; Maynor, B.; Buldum, A.; Lu, J. P.; Liu, J. *J. Phys. Chem. B* **2000**, *28*, 6505.

(33) (a) Somorjai, G. A. *Chemistry in Two Dimensions*: *Surfaces*; Cornel University Press: New York, 1981. (b) Strongin, D. R.; Carrazza, J.; Bare, S. R.; Somorjai, G. A. *J. Catal*. **1987**, *103*, 213.

(34) Huczko, A. *Appl. Phys. A* **2002**, *74*, 617.

(35) Kitiyanan, B.; Alvarez, W. E.; Harwell, J. H.; Resasco, D. E. *Chem. Phys. Lett*. **2000**, *317*, 493.